ELSEVIER

Journal of Alloys and Compounds 388 (2005) 6–14

Journal of ALLOYS AND COMPOUNDS

www.elsevier.com/locate/jallcom

A magnetic and Mössbauer spectral study of $SmFe_{11}Ti$, $LuFe_{11}Ti$, and their respective hydrides

Cristina Piquer[a], Fernande Grandjean[a,*], Gary J. Long[b], Olivier Isnard[c]

[a] *Department of Physics, B5, University of Liège, B-4000 Sart-Tilman, Belgium*
[b] *Department of Chemistry, University of Missouri-Rolla, Rolla, MO 65409-0010, USA*
[c] *Laboratoire de Cristallographie, CNRS, Associé à l'Université J. Fourier, BP 166X, F-38042 Grenoble Cedex, France*

Received 17 June 2004; received in revised form 30 June 2004; accepted 30 June 2004

Abstract

ac Magnetic susceptibility measurements have been carried out on $LuFe_{11}Ti$ and $LuFe_{11}TiH$ and reveal the absence of any spin-reorientation between 4.5 and 293 K. Iron-57 Mössbauer spectral measurements between 4.2 and 295 K have been carried out on $SmFe_{11}Ti$ and $LuFe_{11}Ti$ and their respective hydrides, $SmFe_{11}TiH$ and $LuFe_{11}TiH$. The Mössbauer spectra have been analyzed with a model that considers both the orientation of the iron magnetic moments and the distribution of titanium atoms in the near neighbor environment of the three crystallographically distinct iron sites. The assignment and the temperature dependence of the hyperfine fields are in complete agreement with the unit cell volume and its expansion upon hydrogenation and with those observed in the related $RFe_{11}Ti$ and $RFe_{11}TiH$ compounds. The site assignments and their temperature dependencies of the isomer shifts are in complete agreement both with the Wigner–Seitz cell volumes of the inequivalent iron sites and the crystallographic changes upon hydrogen insertion.

Keywords: Mössbauer spectroscopy; Magnetic measurements; Hydrogenation; Rare-earth intermetallic compounds

1. Introduction

Among the $RFe_{11}Ti$ compounds, where R is a rare earth, that crystallize in the $ThMn_{12}$ *I*4/*mmm* tetragonal structure [1–8], $SmFe_{11}Ti$, $GdFe_{11}Ti$, and $LuFe_{11}Ti$ exhibit [9] an axial magnetic anisotropy, an anisotropy, which is preserved [8–12] in their hydrides. The same behavior is observed [13] in $CeFe_{11}Ti$ and its hydride. In the $RFe_{11}Ti$ compounds, the iron sublattices favor the axial magnetic anisotropy, an anisotropy that is reinforced by the samarium uniaxial magnetocrystalline anisotropy in $SmFe_{11}Ti$ and is further increased [8,14] by the insertion of hydrogen to form $SmFe_{11}TiH$, as is indicated by an increase in the K_1 anisotropy constant from 3.9 to 4.7 MJ/m^3. In contrast, gadolinium, which has no orbital moment because of a half-filled 4f shell, does not reinforce the axial magnetic anisotropy; both $GdFe_{11}Ti$ and $GdFe_{11}TiH$ exhibit a small K_1 anisotropy constant of 1.5 MJ/m^3. Lutetium, like gadolinium has no orbital moment because of a filled 4f shell, and the anisotropy constants [15] of $LuFe_{11}Ti$ and $LuFe_{11}TiH$ are 1.92 and 2.13 MJ/m^3, respectively. In this case, the anisotropy is again dominated by the iron sublattices. The small increase in the K_1 anisotropy constant upon hydrogenation presumably results [15] from an increase in iron magnetic moment that is associated with the unit-cell expansion.

We have carried out a systematic Mössbauer spectral study of the $RFe_{11}Ti$ compounds, [16–22] between 4.2 and 295 K. In all these compounds, the rare-earth atom carries a magnetic moment and contributes to the hyperfine fields measured in the iron-57 Mössbauer spectra. In contrast, in $LuFe_{11}Ti$, the lutetium does not carry a magnetic moment and, hence, the iron hyperfine fields result only from the iron magnetic moments. Hence, it is interesting to investigate this compound by Mössbauer spectroscopy in order to separate the effects of the rare-earth sublattices from those of the iron sublattices.

* Corresponding author.
E-mail address: fgrandjean@ulg.ac.be (F. Grandjean).

0925-8388/$ – see front matter © 2004 Published by Elsevier B.V.
doi:10.1016/j.jallcom.2004.06.073

In this paper, we report and analyze the iron-57 Mössbauer spectra of both $SmFe_{11}Ti$ and $LuFe_{11}Ti$ and their hydrides with the goal of comparing the effect of a magnetic and a non-magnetic rare-earth atom on the magnetic properties of the iron sublattices.

2. Experimental

$SmFe_{11}Ti$ and $LuFe_{11}Ti$ have been synthesized and their hydrogenation was carried out as described earlier [8]. Gravimetric mass-gain analysis indicates that the accuracy of the hydrogen content in the hydrides is ±0.1 per formula unit.

The ac magnetic susceptibilities have been measured on a computer controlled mutual inductance susceptometer [23] at a frequency of 120 Hz in an exciting field of 10^{-4} T. A lock-in amplifier was used to determine the complex susceptibility, $\chi_{ac} = \chi' - j\chi''$, where χ' is the initial susceptibility, a susceptibility that is related to the changes in the sample magnetization, and χ'' is non-zero if magnetic energy is absorbed by the sample.

The Mössbauer spectra were measured between 4.2 and 295 K on a constant-acceleration spectrometer, which utilized a rhodium matrix cobalt-57 source and was calibrated at room temperature with α-iron foil. The Mössbauer spectral absorbers contained 35 mg/cm^2 of powdered sample which had been sieved to a 0.045 mm or smaller diameter particle size. The low temperature spectra were obtained in a Janis Super-Varitemp cryostat and the temperature was controlled with a Lakeshore Cryogenics temperature controller with an accuracy of better than 1% of the observed temperature. The resulting spectra have been fit as discussed below and the estimated errors are at most ±0.2 T for the hyperfine fields and their changes per additional titanium near neighbor, ±0.01 mm/s for the isomer shifts and their changes, and ±0.02 mm/s for the quadrupole shifts and their changes. The observed line widths were between 0.36 and 0.39 mm/s.

3. Structural and magnetic studies

The powder X-ray diffraction patterns of $SmFe_{11}Ti$, $SmFe_{11}TiH$, $LuFe_{11}Ti$, and $LuFe_{11}TiH$ indicate that they crystallize with the tetragonal *I*4/*mmm* $ThMn_{12}$ structure. The lattice parameters are summarized in Table 1. The lattice parameters are in agreement with earlier measurements [24] and are typical of the $RFe_{11}Ti$ compounds with the expected, essentially constant, *c*/*a* ratio of 0.56 and the typical unit cell volume expansion of ca. 3 Å^3 upon hydrogenation. The significant decrease in the lattice parameters in going from the Sm to the Lu compounds is expected and is a consequence of the lanthanide contraction.

The magnetic properties of $SmFe_{11}Ti$, $SmFe_{11}TiH$, $LuFe_{11}Ti$, and $LuFe_{11}TiH$, which are also summarized in Table 1, are typical of these compounds and show the expected ca. 10% increase in the Curie temperature.

There are some significant differences between the lattice parameters and Curie temperatures of the samples measured herein and those reported by Nikitin et al. [24] These differences no doubt result from slight differences in the titanium and/or the hydrogen content of the two sets of samples. For instance, the previously observed [24] lower Curie temperatures of $LuFe_{11}Ti$ and $LuFe_{11}TiH$ probably result from a lower titanium and/or hydrogen content than in the samples studied herein. The difference between the unit-cell volume increase upon hydrogenation of $SmFe_{11}Ti$ and $LuFe_{11}Ti$ reported in Table 1 and those previously reported [24] also results from differences in titanium and hydrogen content.

The ac magnetic susceptibility and high field magnetization studies between 4.5 and 300 K of the same samples of $SmFe_{11}Ti$ and $SmFe_{11}TiH$ as used herein have been reported [8] earlier. This earlier investigation has indicated the absence of any magnetic transitions in either compound and confirms that the easy axis of magnetization is parallel with the tetragonal c-axis of the unit cell between 4 and 300 K.

The temperature dependence of the real component, χ', and the imaginary component, χ'', in the ac susceptibility of $LuFe_{11}Ti$ and $LuFe_{11}TiH$ is shown in Fig. 1. The absence of any sharp transition in, χ'', is an excellent indication of the absence of any spin-reorientations in these samples upon cooling, an observation that is, both expected and consistent with the Stevens coefficients of Lu. The broad changes in both the $\chi'$and χ'' components of the ac susceptibility of $LuFe_{11}Ti$ and $LuFe_{11}TiH$, observed between ca. 150 and 250 K are reminiscent of the magnetic after effects already observed in several intermetallic compounds, such as $CeFe_2$ [25] and $R_2Fe_{14}B$ [26] and analyzed in detail by Monner et al. [27].

Table 1
Lattice parameters and magnetic properties

Compound	*a* (Å)	*c* (Å)	*c*/*a*	*V* (Å^3)	T_c (K)	M_{sat} (μ_B) at 300 K	M_{sat} (μ_B) at 5 K
$SmFe_{11}Ti$	8.558 (1)	4.789 (1)	0.556	350.8 (2)	591	17.3	19.3
$SmFe_{11}TiH$	8.573 (2)	4.808 (1)	0.561	353.4 (3)	634	18.2	19.3
Inc.	0.015	0.019	–	2.6	43	0.9	0.0
%Inc.	0.18	0.40	–	0.74	7.3	5.20	0.0
$LuFe_{11}Ti$	8.462 (1)	4.779 (1)	0.565	342.2 (2)	498	15.2	16.0
$LuFe_{11}TiH$	8.501 (2)	4.783 (1)	0.563	345.7 (3)	558	15.3	17.15
Inc.	0.039	0.004	–	3.5	60	0.1	1.15
%Inc.	0.46	0.08	–	1.02	12.0	0.66	7.19

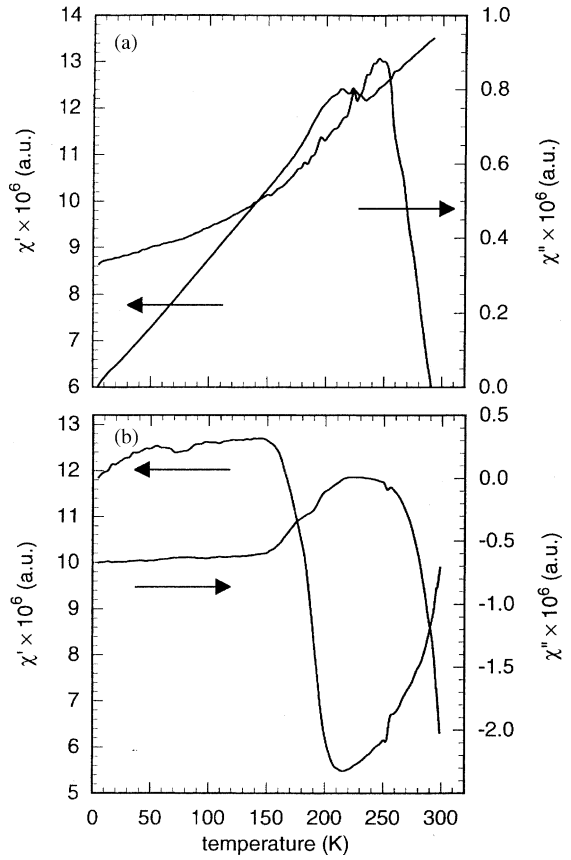

Fig. 1. The temperature dependence of the ac magnetic susceptibility of $LuFe_{11}Ti$ (a) and $LuFe_{11}TiH$ (b).

4. Mössbauer spectral studies

The Mössbauer spectra of $SmFe_{11}Ti$ and $LuFe_{11}Ti$ and their respective hydrides, obtained between 4.2 and 295 K are shown in Figs. 2 and 3, respectively.

In all four of the compounds under study, the iron occupies three crystallographically inequivalent sites, the 8f, 8i, and 8j sites whereas titanium occupies only the 8i sites. Thus, three sextets assigned to the 8f, 8i, and 8j sites, with relative areas in the ratio of 8:6:8 are required to fit the spectra. However, as already observed for many related [16–22] $RFe_{11}Ti$ compounds and their hydrides, these three sextets must be further subdivided because of the random distribution of the titanium, which is a near neighbor to each of the three iron sites. Hence, based on a binomial distribution, the 8i sextet is subdivided into three component sextets with 6.47, 10.79, and 9.98% areas, whereas each of the 8f and 8j sextets is subdivided into three component sextets with 11.51, 15.34, and 9.52% areas; these sextets correspond, respectively, to iron with zero, one, and two or more titanium near neighbors. Thus, at least for compounds exhibiting a uniaxial magnetic structure, nine sextets, with their areas constrained to the above relative values, are required to model the Mössbauer spectra shown in Figs. 2 and 3.

Three hyperfine parameters define each of the above sextets, the magnetic hyperfine field, H, the isomer shift, δ, and the quadrupole shift, ε. In order to both reduce the number of variables and to build in constraints into the model, it has been assumed herein that the three hyperfine parameters for each inequivalent iron site will vary linearly with n, the number of titanium near neighbors, such that

$$H_n = H_0 + n\Delta H,$$

$$\delta_n = \delta_0 + n\Delta\delta,$$

and

$$\varepsilon_n = \varepsilon_0 + n\Delta\varepsilon,$$

where H_0, δ_0, and ε_0 are, respectively, the magnetic hyperfine field, isomer shift, and quadrupole shift, corresponding to zero titanium near neighbors and ΔH, $\Delta\delta$, and $\Delta\varepsilon$, are the respective changes observed for one additional titanium near neighbor. A similar linear dependence of the hyperfine field on n has been successful in our earlier [28–31] analyses of the Mössbauer spectra of a variety of $R_2Fe_{17-x}M_x$ solid solutions. This model, has led to the components and the fits shown in Figs. 2 and 3, includes 18 hyperfine parameters, one line width, and one total absorption area. The resulting hyperfine parameters are given in Tables 2–5.

One would expect that the large number of fitting parameters should easily lead to good but perhaps far from unique fits. Hence, to give added confidence to our spectral analysis we use the temperature dependencies of the hyperfine parameters to both improve upon the uniqueness of our fits and to provide a further physical constraint upon the fits. Past experience indicates that it is not as easy to obtain good fits of the observed spectra as might be anticipated, especially when physically viable changes in the hyperfine parameters with temperature are imposed upon the fits. Thus, so far we have not been able to find an alternative model that both provides good fits and viable changes in the hyperfine parameters with temperature, but such an undiscovered model may, of course, exist.

5. Discussion

5.1. Hyperfine fields

The assignment along with the temperature dependence of the three hyperfine fields for zero titanium near neighbor and their weighted average for $SmFe_{11}Ti$ and $LuFe_{11}Ti$ and their respective hydrides, are shown in Figs. 4 and 5, respectively. The Wigner–Seitz cell [32] of the three inequivalent iron sites in $RFe_{11}Ti$ and $RFe_{11}TiH$ has been used to show that the 8i site has 11.75 iron near neighbors, the largest average number of iron near neighbors. In contrast, the 8f and 8j iron sites each have only nine iron near neighbors. Thus, on the basis of both the number of near-neighbor ions and its relative area, the sextet with the largest hyperfine field, H_0, has been assigned

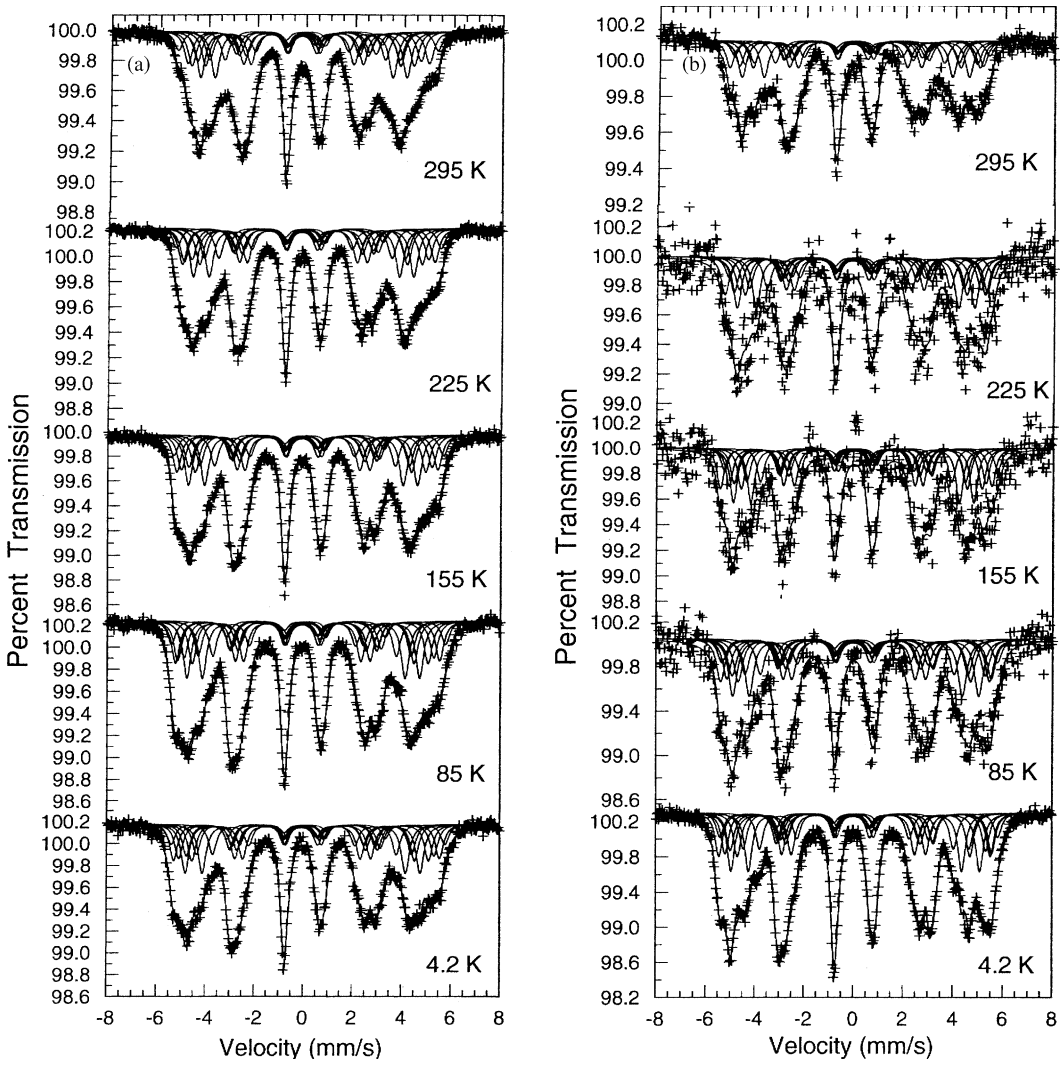

Fig. 2. The Mössbauer spectra of $SmFe_{11}Ti$ (a) and $SmFe_{11}TiH$ (b) obtained at the indicated temperatures.

to the 8i site, an assignment that is further supported by the observed isomer shift values, see below.

The assignment of the remaining two sites is more difficult because of both their identical constrained percentage areas and their identical iron near neighbor environments. As a consequence, because it is not possible to unequivocally assign the 8f and 8j sextets on the basis of their fields or relative areas, their assignment is determined by their differing isomer shifts as is explained below. The resulting assignment of the fields to the three iron sites is identical to that previously used [33] for the $SmFe_{11-x}Co_x$ compounds and the site average fields fitted in ref. [33] are smaller than the maximum fields reported in Table 2. Although the three H_0 hyperfine fields increase upon hydrogenation, the sequence of hyperfine fields, 8i > 8j > 8f, remains unchanged as is shown in Figs. 4 and 5. In addition to the lattice expansion upon hydrogenation, a Wigner–Seitz cell analysis [32] indicates that only the 8j site has a hydrogen near neighbor; neither the 8f nor the 8i sites have any hydrogen near neighbors.

The solid lines shown in Figs. 4 and 5 are Brillouin curves for spin 5/2; all the hyperfine fields follow these Brillouin curves. The hyperfine fields observed in $SmFe_{11}Ti$ and $SmFe_{11}TiH$ (Tables 2–5), are larger by 3–4 T than those observed in $LuFe_{11}Ti$ and $LuFe_{11}TiH$. This difference in hyperfine fields indicates the importance of the contribution of the magnetic moment carried by samarium.

The increase in the average hyperfine fields upon hydrogenation is ca. 1 and 2 T at 4.2 K, as is shown in Figs. 4 and 5 for $SmFe_{11}Ti$ and $LuFe_{11}Ti$, respectively. Similar increases in the hyperfine fields upon hydrogenation or nitrogenation of several R_2Fe_{17} and $RFe_{11}Ti$ compounds have been observed [16–22,28–31]. This increase in hyperfine field results in part from the increase in unit cell volume upon hydrogenation and the larger increase observed for $LuFe_{11}Ti$ results from the larger relative increase in unit-cell volume as is indicated in Table 1. The nearly temperature independent decreases in the hyperfine field per titanium near neighbor are between −1.5

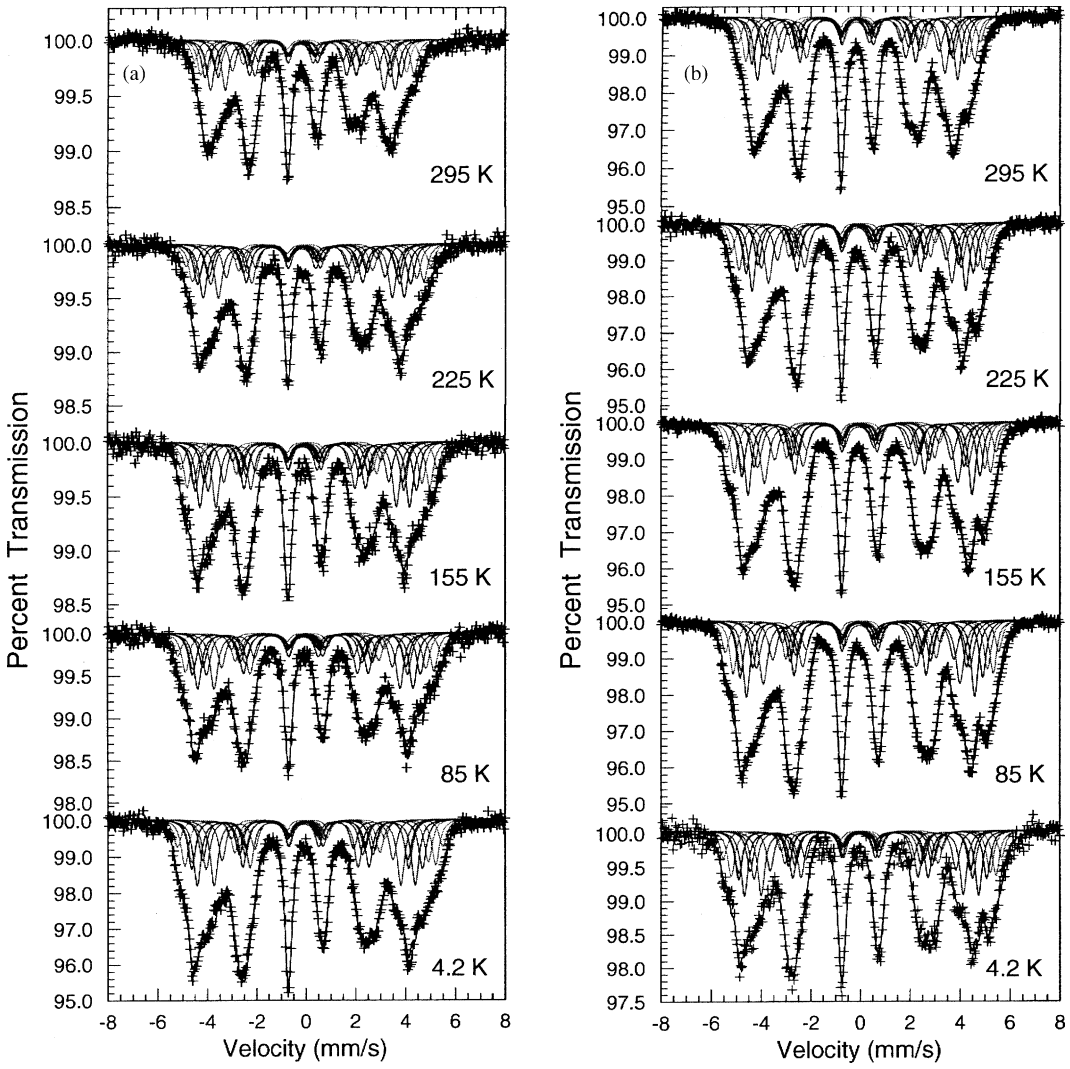

Fig. 3. The Mössbauer spectra of $LuFe_{11}Ti$ (a) and $LuFe_{11}TiH$ (b) obtained at the indicated temperatures.

and −2.8 T for the three sites and are very similar to those observed [16–22,34] in the other $RFe_{11}Ti$ compounds and their respective hydrides and are within the range from −1.1 to −6 T observed [35,36] in a spinel oxide and in $Nd_2Fe_{16}Ti$, respectively.

5.2. Isomer shifts

The assignment and the temperature dependence of the three site average isomer shifts, and their weighted average, for $SmFe_{11}Ti$ and $LuFe_{11}Ti$ and their respective hydrides, are shown in Figs. 6 and 7, respectively. The site average isomer shifts have been calculated from the δ_n values weighted with the percent contribution given by the binomial distribution. In agreement with the Wigner–Seitz cell analysis [32] of the three inequivalent iron sites, the sequence of isomer shifts, 8i > 8j > 8f, follows the sequence of Wigner–Seitz cell volumes. Such a relationship between isomer shifts and Wigner–Seitz cell volumes has been observed [28,37] in many R_2Fe_{17} compounds and [16–22] in the other $RFe_{11}Ti$ and their hydrides. The overall increase in unit-cell volume accounts for the increase in the weighted average isomer shift upon hydrogenation. Further, the isomer shifts are smaller in $LuFe_{11}Ti$ and its hydride, than in $SmFe_{11}Ti$ and its hydride, in agreement with the smaller unit cell volume observed in $LuFe_{11}Ti$ and its hydride. Finally, the 8i isomer shift does not substantially increase upon hydrogenation. This smaller increase is to be compared with a decrease [22] in the 8i isomer shift upon hydrogenation of $GdFe_{11}Ti$ to form $GdFe_{11}TiD$.

The temperature dependence of the weighted average isomer shift in $SmFe_{11}Ti$ and $LuFe_{11}Ti$ and their respective hydrides, shown in Figs. 6 and 7, has been fit [38,39] with the Debye model for the second order Doppler shift. The resulting effective vibrating mass [39] is 57 g/mol and the effective Mössbauer temperatures are 383, 402, 371, and 420 K, for $SmFe_{11}Ti$, $SmFe_{11}TiH$, $LuFe_{11}Ti$, and $LuFe_{11}TiH$, respectively. These

Table 2
Mössbauer spectral hyperfine parameters for $SmFe_{11}Ti$

Parameter	T (K)	8f	8i	8j	Wt. Av.
H_0 (ΔH) (T)	295	24.8 (−2.2)	31.5 (−1.8)	28.2 (−1.8)	25.8
	225	26.2 (−2.2)	33.5 (−1.7)	30.3 (−1.7)	27.5
	155	27.4 (−2.2)	34.1 (−1.7)	31.5 (−1.7)	28.5
	85	28.0 (−2.4)	34.6 (−1.5)	31.9 (−1.5)	29.1
	4.2	28.2 (−2.5)	35.0 (−1.6)	32.2 (−1.6)	29.3
δ_0[a] ($\Delta\delta$) (mm/s)	295	−0.167 (0.018)	0.013 (−0.003)	−0.149 (0.012)	−0.102
	225	−0.105 (0.018)	0.085 (−0.003)	−0.095 (0.012)	−0.040
	155	−0.065 (0.016)	0.122 (−0.003)	−0.060 (0.012)	−0.003
	85	−0.038 (0.018)	0.140 (−0.003)	−0.034 (0.012)	0.021
	4.2	−0.029 (0.018)	0.165 (−0.003)	−0.025 (0.012)	0.035
ε_0 ($\Delta\varepsilon$) (mm/s)	295	0.006 (0.054)	0.036 (0.057)	−0.044 (0.051)	0. 050
	225	0.035 (0.045)	0.085 (0.065)	−0.090 (0.090)	0.069
	155	0.031 (0.034)	0.083 (0.081)	−0.142 (0.116)	0.059
	85	0.028 (0.026)	0.089 (0.032)	−0.086 (0.097)	0.055
	4.2	0.071 (0.016)	0.068 (0.095)	−0.112 (0.071)	0.072

[a] Relative to room temperature α-iron foil.

Table 3
Mössbauer spectral hyperfine parameters for $SmFe_{11}TiH$

Parameter	T (K)	8f	8i	8j	Wt. Av.
H_0 (ΔH) (T)	295	26.1 (−2.4)	32.1 (−1.4)	31.4 (−2.8)	27.4
	225	27.8 (−2.4)	33.5 (−1.4)	32.6 (−2.8)	28.8
	155	28.8 (−2.4)	34.3 (−1.4)	33.2 (−2.8)	29.6
	85	29.0 (−2.4)	34.5 (−1.4)	33.7 (−2.8)	29.9
	4.2	29.2 (−2.4)	34.8 (−1.4)	34.0 (−2.8)	30.2
δ_0[a] ($\Delta\delta$) (mm/s)	295	−0.078 (0.031)	0.076 (−0.019)	−0.040 (−0.002)	−0.018
	225	−0.045 (0.031)	0.115 (−0.019)	−0.001 (−0.002)	0.019
	155	−0.020 (0.031)	0.135 (−0.019)	0.030 (−0.002)	0.045
	85	−0.002 (0.031)	0.150 (−0.019)	0.045 (−0.002)	0.061
	4.2	−0.002 (0.031)	0.152 (−0.019)	0.047 (−0.002)	0.062
ε_0 ($\Delta\varepsilon$) (mm/s)	295	0.152 (0.055)	0.231 (0.006)	−0.050 (0.073)	0.146
	225	0.120 (0.055)	0.200 (0.006)	−0.045 (0.073)	0.125
	155	0.080 (0.055)	0.160 (0.006)	−0.040 (0.073)	0.104
	85	0.030 (0.055)	0.120 (0.006)	−0.030 (0.073)	0.079
	4.2	0.020 (0.055)	0.105 (0.006)	−0.021 (0.073)	0.074

[a] Relative to room temperature α-iron foil.

Table 4
Mössbauer spectral hyperfine parameters for $LuFe_{11}Ti$

Parameter	T (K)	8f	8i	8j	Wt. Av.
H_0 (ΔH) (T)	295	21.6 (−1.7)	28.4 (−1.7)	24.5 (−1.5)	22.9
	225	23.6 (−1.9)	30.6 (−1.7)	26.7 (−1.5)	25.0
	155	24.5 (−1.9)	32.0 (−1.8)	27.7 (−1.4)	26.0
	85	25.2 (−1.9)	33.0 (−1.9)	28.5 (−1.5)	26.7
	4.2	25.4 (−1.9)	33.2 (−1.8)	28.8 (−1.7)	26.9
δ_0[a] ($\Delta\delta$) (mm/s)	295	−0.156 (0.008)	0.014 (−0.026)	−0.111 (−0.028)	−0.107
	225	−0.110 (0.001)	0.050 (−0.023)	−0.069 (−0.023)	−0.066
	155	−0.070 (0.002)	0.073 (−0.018)	−0.029 (−0.025)	−0.029
	85	−0.040 (0.002)	0.101 (−0.017)	−0.001 (−0.026)	0.000
	4.2	−0.030 (0.002)	0.106 (−0.012)	0.010 (−0.025)	0.010
ε_0 ($\Delta\varepsilon$) (mm/s)	295	0.131 (0.022)	0.115 (0.001)	−0.057 (0.040)	0.079
	225	0.103 (0.021)	0.067 (0.028)	−0.051 (0.012)	0.057
	155	0.114 (0.010)	0.087 (−0.010)	0.037 (−0.041)	0.064
	85	0.127 (−0.004)	0.084 (0.017)	0.004 (−0.029)	0.065
	4.2	0.130 (−0.002)	0.086 (0.019)	0.025 (−0.021)	0.077

[a] Relative to room temperature α-iron foil.

Table 5
Mössbauer spectral hyperfine parameters for $LuFe_{11}TiH$

Parameter	T (K)	8f	8i	8j	Wt. Av.
H_0 (ΔH) (T)	295	23.3 (−1.8)	30.0 (−1.7)	26.5 (−1.5)	24.7
	225	24.9 (−1.9)	32.1 (−1.6)	28.3 (−1.6)	26.4
	155	26.2 (−2.1)	33.6 (−1.7)	29.7 (−1.7)	27.7
	85	26.6 (−2.0)	34.1 (−1.7)	30.3 (−1.8)	28.2
	4.2	27.3 (−2.0)	34.7 (−1.7)	31.0 (−1.7)	28.8
δ_0[a] ($\Delta\delta$) (mm/s)	295	−0.133 (0.011)	−0.068 (0.015)	−0.101 (−0.018)	−0.101
	225	−0.064 (0.002)	−0.004 (0.004)	−0.040 (−0.027)	−0.046
	155	−0.018 (0.007)	0.036 (0.010)	0.007 (−0.028)	0.002
	85	−0.005 (0.001)	0.050 (0.019)	0.025 (−0.024)	0.022
	4.2	0.005 (0.001)	0.063 (0.020)	0.035 (−0.024)	0.033
ε_0 ($\Delta\varepsilon$) (mm/s)	295	0.201 (−0.011)	−0.002 (0.058)	−0.020 (0.007)	0.082
	225	0.186 (0.016)	−0.020 (0.073)	0.006 (0.000)	0.092
	155	0.215 (0.001)	−0.001 (0.070)	0.025 (−0.008)	0.106
	85	0.228 (−0.016)	0.032 (0.052)	0.043 (−0.021)	0.111
	4.2	0.212 (−0.033)	0.045 (0.037)	0.094 (−0.050)	0.107

[a] Relative to room temperature α-iron foil.

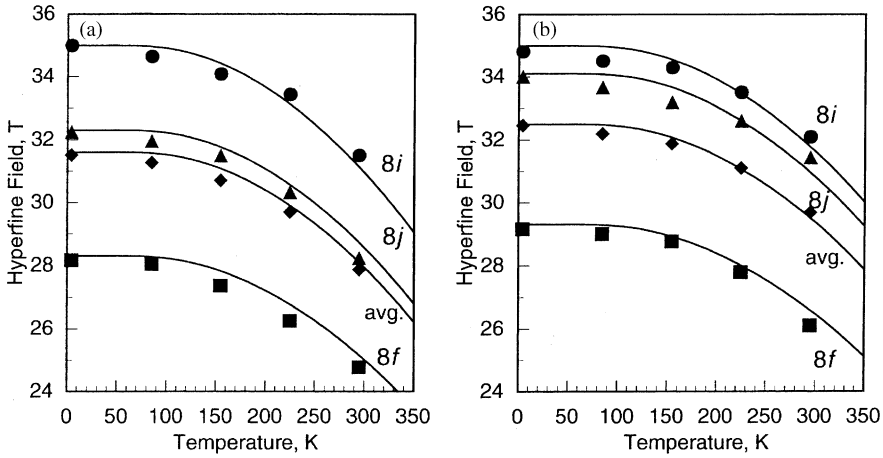

Fig. 4. The temperature dependence of the maximum hyperfine fields, H_0, at the three iron sites, and their average, in $SmFe_{11}Ti$ (a) and $SmFe_{11}TiH$ (b). The solid lines are the result of fits with a Brillouin function with $S = 5/2$.

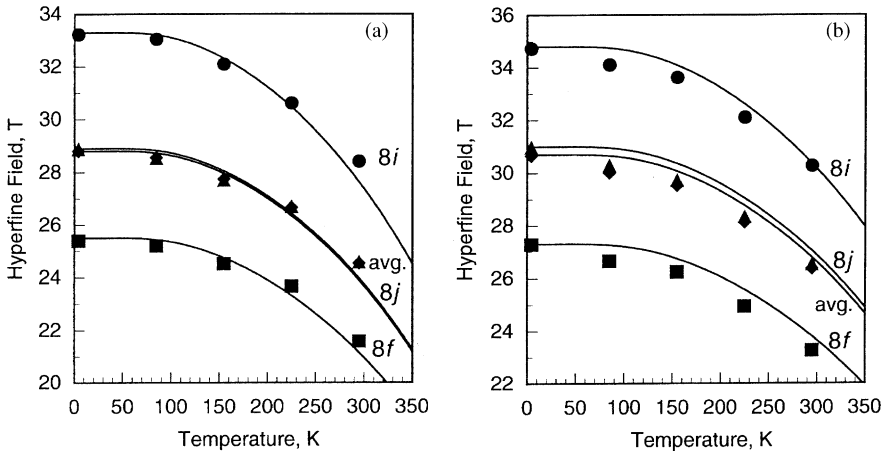

Fig. 5. The temperature dependence of the maximum hyperfine fields, H_0, at the three iron sites, and their average, in $LuFe_{11}Ti$ (a) and $LuFe_{11}TiH$ (b). The solid lines are the result of fits with a Brillouin function with $S = 5/2$. The hyperfine fields of the 8j site and the weighted average are essentially identical in $LuFe_{11}Ti$ and are very similar in $LuFe_{11}TiH$.

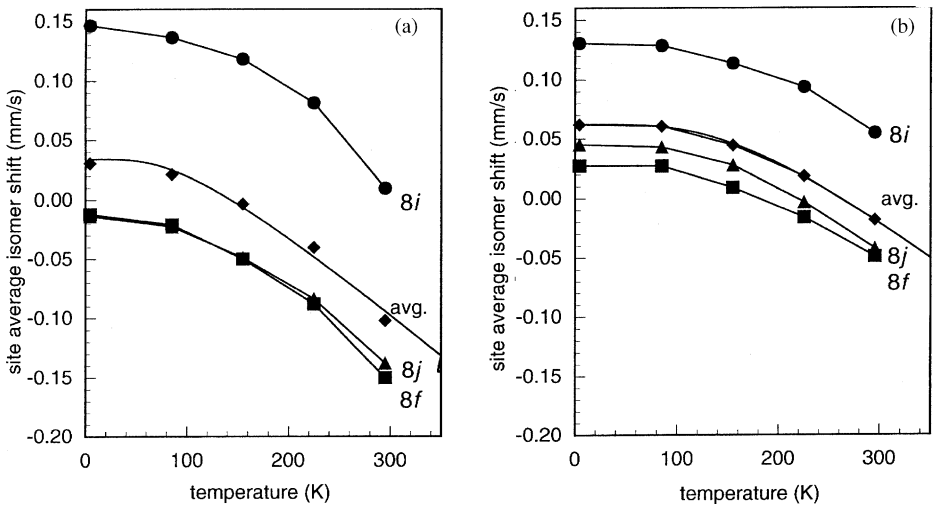

Fig. 6. The temperature dependence of the three site average isomer shifts, and their average, in $SmFe_{11}Ti$ (a) and $SmFe_{11}TiH$ (b). The isomer shifts of the 8j and 8f sites are close to identical in $SmFe_{11}Ti$. The solid line shown for the average value is the result of the second-order Doppler shift fit discussed in the text.

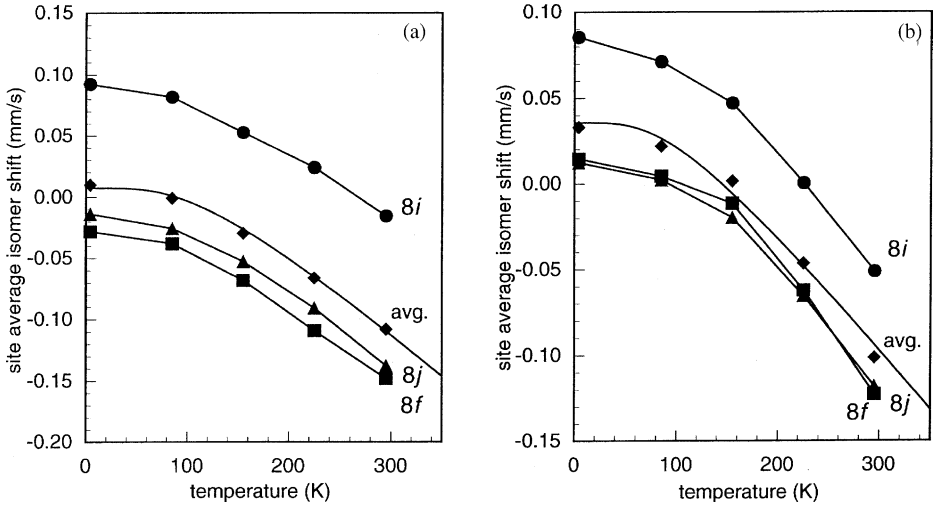

Fig. 7. The temperature dependence of the three site average isomer shifts, and their average, in $LuFe_{11}Ti$ (a) and $LuFe_{11}TiH$ (b). The solid line shown for the average value is the result of the second-order Doppler shift fit discussed in the text.

temperatures, which are determined with an accuracy of ca. 10 K are typical [37,40] of intermetallic compounds.

5.3. Quadrupole shifts

The sign of the average quadrupole shift observed in the spectra of the $RFe_{11}Ti$ and their hydrides was found [17] to reflect the direction of the easy magnetization axis. The positive average quadrupole shifts of 0.07–0.10 mm/s observed herein are in complete agreement with the uniaxial magnetization axis in $SmFe_{11}Ti$ and $LuFe_{11}Ti$ and their respective hydrides. Similarly, in $GdFe_{11}Ti$ and its hydride, which both show uniaxial magnetic anisotropy, positive average quadrupole shifts are observed [22].

6. Conclusions

From a macroscopic point of view the insertion of hydrogen into $SmFe_{11}Ti$ and $LuFe_{11}Ti$ expands the lattice and, as expected, increases the Curie temperature. From a microscopic point of view, the insertion of hydrogen increases the three hyperfine fields and the 8f and 8j isomer shifts, as a result of lattice expansion. The larger increases in hyperfine field observed upon hydrogenation of $LuFe_{11}Ti$ are consistent with the larger increase in unit-cell volume. The smaller isomer shifts observed in $LuFe_{11}Ti$ and $LuFe_{11}TiH$ are consistent with the smaller unit-cell volumes as compared with those of $SmFe_{11}Ti$ and $SmFe_{11}TiH$. The smaller hyperfine fields observed in $LuFe_{11}Ti$ and $LuFe_{11}TiH$ as compared with those of $SmFe_{11}Ti$ and $SmFe_{11}TiH$ are a consequence

of the absence of magnetic moment on Lu. Further, virtually identical spectra and hyperfine fields are observed [13] for $LuFe_{11}Ti$ and $LuFe_{11}TiH$, and $CeFe_{11}Ti$ and $CeFe_{11}TiH$, respectively.

Acknowledgments

The authors thank Dr. R.P. Hermann and Ms. L. Rebbouh for their assistance in obtaining the Mössbauer spectra. The financial support of the University of Liège through Grant No. 2850006 is acknowledged with thanks. This work was partially supported by the US National Science Foundation through Grant INT-9815138, and the "Centre National de la Recherche Scientifique, France" through Grant Action Initiative No. 7418.

References

[1] A. Apostolov, R. Bezdushnyi, N. Stanev, R. Damianova, D. Fruchart, O. Isnard, J.L. Soubeyroux, J. Alloys Compd. 253–254 (1997) 318–321.
[2] A. Apostolov, R. Bezdushnyi, N. Stanev, R. Damianova, D. Fruchart, J.L. Soubeyroux, O. Isnard, J. Alloys Compd. 265 (1998) 1–5.
[3] E.B. Boltich, B.M. Ma, L.Y. Zhang, F. Pourarian, S.K. Malik, S.G. Sankar, W.E. Wallace, J. Magn. Magn. Mater. 78 (1989) 365.
[4] B.P. Hu, H.S. Li, J.P. Gavigan, J.M.D. Coey, J. Phys. Condens. Matter 1 (1989) 755.
[5] X.C. Kou, T.S. Zhao, R. Grössinger, H.R. Kirchmayer, X. Li, F.R. de Boer, Phys. Rev. B 47 (1993) 3231.
[6] V.K. Sinha, S.K. Malik, D.T. Adroja, J. Elbicki, S.G. Sankar, W.E. Wallace, J. Magn. Magn. Mater. 80 (1989) 281.
[7] L.Y. Zhang, E.B. Boltich, V.K. Sinha, W.E. Wallace, IEEE Trans. Magn. 25 (1989) 3303.
[8] O. Isnard, M. Guillot, S. Miraglia, D. Fruchart, J. Appl. Phys. 79 (1996) 5542.
[9] S.A. Nikitin, I.S. Tereshina, V.N. Verbetsky, A.A. Salamova, J. Alloys Compd. 316 (2001) 46.
[10] O. Isnard, J. Alloys Compd. 356–357 (2003) 17.
[11] O. Isnard, M. Guillot, J. Appl. Phys. 83 (1998) 6730–6732.
[12] O. Isnard, P. Vulliet, J.P. Sanchez, D. Fruchart, J. Magn. Magn. Mater. 189 (1998) 47.
[13] G.J. Long, D. Hautot, F. Grandjean, O. Isnard, S. Miraglia, J. Magn. Magn. Mater. 202 (1999) 100.
[14] O. Isnard, S. Miraglia, M. Guillot, D. Fruchart, J. Alloys Compd. 275–277 (1998) 637.
[15] I.S. Tereshina, S.A. Nikitin, N.Yu. Pankratov, G.A. Bezkorovajnaya, A.A. Salamova, V.N. Verbetsky, T. Mydlarz, Yu.V. Skourski, J. Magn. Magn. Mater. 231 (2001) 213.
[16] C. Piquer, F. Grandjean, O. Isnard, V. Pop, G.J. Long, J. Alloys Compd. 377 (2004) 1–7.
[17] C. Piquer, F. Grandjean, O. Isnard, V. Pop, G.J. Long, J. Appl. Phys. 95 (2004) 6308.
[18] C. Piquer, F. Grandjean, O. Isnard, G.J. Long, J. Alloys Compd. 353 (2003) 33.
[19] C. Piquer, F. Grandjean, O. Isnard, G.J. Long, J. Appl. Phys. 93 (2003) 3414.
[20] C. Piquer, R.P. Hermann, F. Grandjean, O. Isnard, G.J. Long, J. Phys. Condens. Matter 15 (2003) 7395.
[21] C. Piquer, F. Grandjean, O. Isnard, G.J. Long, J. Magn. Magn. Mater. 265 (2003) 156.
[22] C. Piquer, F. Grandjean, O. Isnard, G.J. Long, J. Magn. Magn. Mater. 263 (2003) 235.
[23] C. Rillo, F. Lera, A. Badia, L. Angurel, J. Bartolomé, F. Palacio, R. Navarro, A.J. Duyneveldt, in: R.A. Hein, J.L. Francavilla, D.H. Liebenberg (Eds.), Susceptibility of Superconductors and Other Spin Systems, Plenum Press, New York, 1992.
[24] S.A. Nikitin, I.S. Tereshina, V.N. Verbetsky, A.A. Salamova, J. Alloys Compd. 316 (2001) 46.
[25] E.H. Büchler, M. Hirscher, H. Kronmüller, in: G.J. Long, F. Grandjean, K.H.J. Buschow (Eds.) Interstitial Intermetallic Alloys, Kluver, Dordrecht, 1994, p. 521;
C.U. Maier, M. Hirscher, H. Kronmüller, Philos. Mag. B Phys. Condens. Matter 63 (1991) 405.
[26] L.M. Garcia, J. Bartolomé, F.J. Lazaro, C. de Fransico, J.M. Munoz, D. Fruchart, J. Magn. Magn. Mater. 140–144 (1995) 1049.
[27] N. Monner, J. van Lier, M. Hirscher, H. Kronmüller, J. Alloys Compd. 270 (1998) 58;
N. Monner, H. Reule, M. Hirscher, H. Kronmüller, Philos. Mag. B Phys. Condens. Matter. 79 (1999) 585.
[28] D. Hautot, G.J. Long, P.C. Ezekwenna, F. Grandjean, D.P. Middleton, K.H.J. Buschow, J. Appl. Phys. 83 (1998) 6736.
[29] G.J. Long, G.K. Marasinghe, S. Mishra, O.A. Pringle, Z. Hu, W.B. Yelon, D.P. Middleton, K.H.J. Buschow, F. Grandjean, J. Appl. Phys. 76 (1994) 5383.
[30] D.P. Middleton, S.R. Mishra, G.J. Long, O.A. Pringle, Z. Hu, W.B. Yelon, F. Grandjean, K.H.J. Buschow, J. Appl. Phys. 78 (1995) 5568.
[31] S.R. Mishra, G.J. Long, O.A. Pringle, D.P. Middleton, Z. Hu, W.B. Yelon, F. Grandjean, K.H.J. Buschow, J. Appl. Phys. 79 (1996) 3145.
[32] L. Gelato, J. Appl. Crystallogr. 14 (1981) 141.
[33] L. Bessais, C. Djega-Mariadassou, J.M. Grenèche, J. Magn. Magn. Mater. 226–230 (2001) 1564.
[34] I.S. Tereshina, P. Gaczynsku, V.S. Rusakov, H. Drulis, S.A. Nikitin, W. Suski, N.V. Tristan, T. Palewski, J. Phys. Condens. Matter 13 (2001) 8161.
[35] J.L. Dormann, Rev. Phys. Appl. 15 (1980) 1113.
[36] F. Grandjean, P.C. Ezekwenna, G.J. Long, O.A. Pringle, Ph. L'Héritier, M. Ellouze, H.P. Luo, W.B. Yelon, J. Appl. Phys. 84 (1998) 1893.
[37] D. Hautot, G.J. Long, F. Grandjean, O. Isnard, Phys. Rev. B 62 (2000) 11731.
[38] G.J. Long, D. Hautot, F. Grandjean, D.T. Morelli, G.P. Meisner, Phys. Rev. B 60 (1999) 7410;
G.J. Long, D. Hautot, F. Grandjean, D.T. Morelli, G.P. Meisner, Phys. Rev. B 62 (2000) 6829.
[39] R.H. Herber, in: R.H. Herber (Ed.), Chemical Mössbauer Spectroscopy, Plenum Press, New York, 1984, p. 199.
[40] G.J. Long, O. Isnard, F. Grandjean, J. Appl. Phys. 91 (2002) 1423.